Numerical study of nanofluid infusion in deformable tissues for hyperthermia cancer treatments

Di Su, Ronghui Ma & Liang Zhu

Medical & Biological Engineering & Computing

ISSN 0140-0118

Med Biol Eng Comput
DOI 10.1007/s11517-011-0819-y

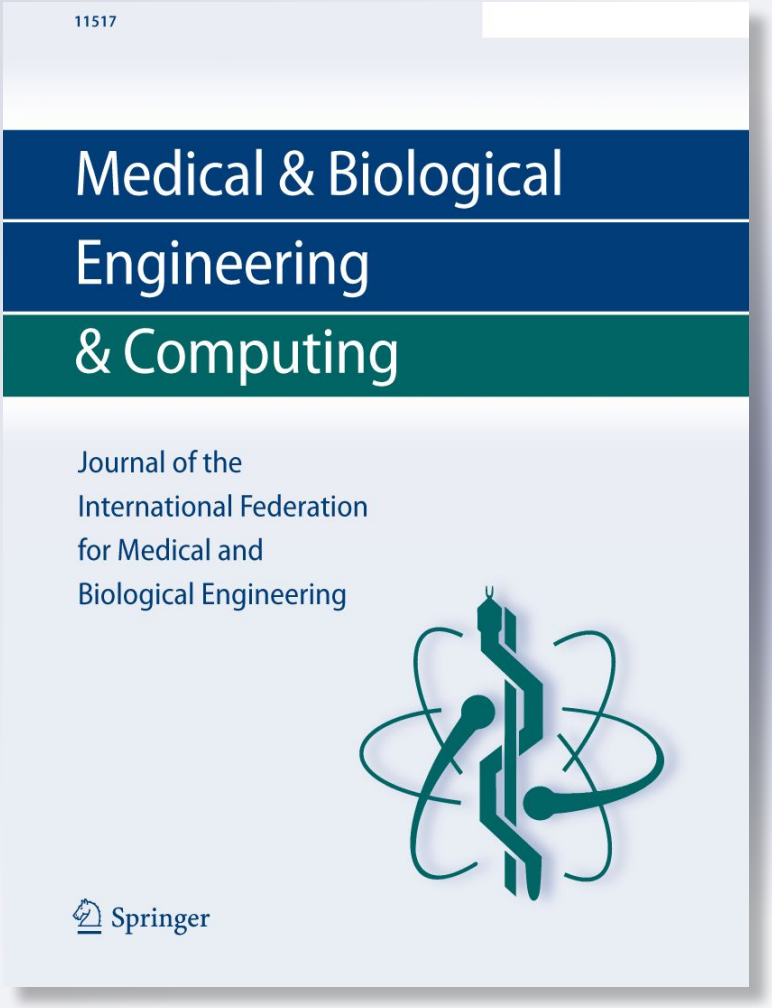

Springer

Med Biol Eng Comput
DOI 10.1007/s11517-011-0819-y

ORIGINAL ARTICLE

Numerical study of nanofluid infusion in deformable tissues for hyperthermia cancer treatments

Di Su · Ronghui Ma · Liang Zhu

Received: 15 February 2011 / Accepted: 31 July 2011

Abstract Direct infusion by means of needles is one of the widely used methods for the delivery of nanoparticles in tumors for hyperthermia cancer treatments. During an infusion process, infusion-induced deformation can substantially affect the dispersion of the nanoparticles injected in a biological tissue. In this study, a poroelastic model is developed to investigate fluid transport and flow-induced tissue deformation in a tumor during an infusion process. A surface tracking technique is employed to predict the shape of nanofluid spreading after injection. The model is then used to simulate the formation of backflow and the change of tissue porosity due to the deformation. Specifically, we quantify the influence of the backflow on the spreading shape of the nanofluid and its dependence on injection parameters such as infusion rates, needle diameters, and tumor elastic properties. It is found that backflow is an important factor causing an irregular distribution of the nanofluid injected in a tumor. A higher infusion rate, larger needle diameter, and lower elastic modulus yield a longer backflow length and cause a more irregular spreading shape of the nanofluid. The infusion-induced tissue deformation also leads to a pore swelling and an increase of the porosity in the vicinity of the needle tip and the needle outer surface. It is anticipated that the increased pore size may facilitate the particle penetration in a tumor. To achieve a controlled heat generation, the injection parameters should be selected judiciously with the consideration of tumor sizes, tumor properties, and thresholds at which tumors break under the infusion pressure.

D. Su · R. Ma (✉) · L. Zhu
Department of Mechanical Engineering, University of Maryland, Baltimore County, Baltimore, MD 21250, USA
e-mail: roma@umbc.edu

Keywords Infusion · Nanoparticle transport · Tissue deformation · Hyperthermia · Backflow

1 Introduction

Nanoparticles have found important applications in various hyperthermia cancer treatments due to their abilities to generate impressive levels of heat when excited by an external magnetic field or laser irradiation [4, 8, 10–12, 16, 17, 23, 28]. For example, magnetic nanoparticles delivered in a tumor can induce localized heating when agitated by an alternating magnetic field. The resulting temperature elevations in the tumor can cause an irreversible thermal damage to the tumor cells [10, 12, 16, 17, 23]. In laser photothermal therapy, where heat is induced by a near-infrared laser irradiation on the tumor surface, the inclusion of gold nanoshells/nanorods in the tumor maximizes the absorption of laser energy, leading to enhanced temperature elevations confined in the target region [4, 8, 28]. Nanoparticles have also been innovatively used in a variety of clinical and biomedical research and applications [20]. Although various types of nanoparticles have demonstrated great potentials in hyperthermia cancer treatment, many challenges need to be addressed before their widespread applications in clinical studies. One leading issue is the limited knowledge of nanoparticles distribution and anticipated temperature elevations in tumors. Since nanoparticles serve as the heating agents, their distributions in a tumor play a critical role in determining the efficacy of the treatment. The lack of control of the nanoparticle distribution may lead to inadequacy in killing tumor cells and/or damage to the healthy tissue.

Intratumoral infusion is an important technique to deliver a variety of nanostructures in tumors by continuous

Published online: 14 August 2011

injection of a nanofluid under a positive pressure gradient [1, 11, 12, 21]. Since it allows those agents to overcome obstacles such as interstitial fluid pressure and brain blood barrier through enhanced convective transport [22], direct infusion is considered the best method available for distributing large therapeutic agents in tumors. Salloum et al. [30] studied the injection of a ferrofluid in semi-transparent agarose gels, and demonstrated that the distribution volume of the ferrofluid is sensitive to both injection rates and gel properties. The study also suggests a non-uniform nanoparticle distribution with a high nanoparticle concentration near the needle tip [30, 33]. In addition, a high infusion rate is more likely to yield an uncontrollable and irregular-shaped nanofluid distribution. The study reveals a qualitative relationship among the injection parameters, gel properties, and the particle distributions; however, the underlying mechanisms that govern the transport of nanofluids in tissues during an infusion are poorly understood. Specifically, it remains unclear to what extent the deformation of the tissue affects the nanoparticle transport in tumors.

Previous studies of drug delivery by direct infusion show that infusion pressures induce the deformation of gels/tissues, and subsequently change the size and connectedness of the aqueous pathways in the porous structure [15, 22]. As a result, the resistance of the porous medium to fluid flow is altered, and the permeability becomes a function of the deformation. Tissue deformation also changes the effective pore size of the extracellular structure, which might either facilitate or hinder the particle penetration [26]. McGuire et al. [22] developed a one-dimensional poroelastic model to explain the nonlinear relation of the infusion rate and infusion pressure due to the heterogeneous tissue deformation. Chen et al. [6] conducted experimental and theoretical studies of the poroelasticity of brain-tissue-equivalent phantom gels to characterize the influence of gel deformation on infusion pressure, gel matrix dilation, and pore fraction. However, this study is limited to soft gels and low infusion rates in the range of 0.5–10 μl min^{-1}. Ivanchenko et al. [14] measured the deformation of brain-tissue-equivalent phantom gels due to fluid infusion for a single infusion rate of 5 μl min^{-1}. The changes in the hydraulic conductivity and the porosity close to the catheter tip were analyzed.

Tissue deformation also causes the infusate to flow back along the needle track, leading to the leakage of the infusate into the surrounding healthy tissue. The backflow has been a challenge for the administration of therapeutic agents to brain tumors through enhanced convection delivery [1]. Morrison et al. [25] derived a simplified relation to quantify the backflow distance as a function of infusion rates and the diameters of catheters. Raghavan et al. [29] further reformulated and developed this analytical model [25]. The simplifications involved in the models do not allow precise prediction of the shapes of the infusate distribution in tissues.

Despite the extensive studies of direct infusion processes, the influence of tissue deformation on the transport of nanofluids in tumors remains poorly understood. Quantitative information on the shape of nanofluid distribution, the change of tumor porosity, and their dependence on injection parameters, is not available. The lack of information on the change of pore size induced by the infusion pressure makes it difficult to assess its influence on nanoparticle penetration. In this study, a poroelastic model considering fluid flow through porous media and flow-induced tissue deformation is developed to investigate the infusion process. A surface tracking technique is employed to predict the shapes of the nanofluid spreading. The model is used to simulate the formation of backflow, and the change of tumor porosity for various combinations of injection parameters and tissue properties. The influence of the backflow on the spreading of the nanofluid, the change of the tissue porosity, and their dependence on the infusion rates, needle diameters, and tumor elastic properties are quantified for infusion rates in the range of 2.5–20 μl min^{-1}.

2 Methods

The poroelastic model for nanofluid infusion in tumors consists of the equations for fluid flow through porous tissues, tissue deformation, bulk flow in the annular space surrounding a needle, and surface tracking of flow front. Since most of the ferrofluids used in the experimental study of magnetic nanoparticle hyperthermia have a low concentration [30, 31, 35], we assume that the nanofluids used in a treatment are dilute with a concentration lower than 5% by volume, where the presence of the particles does not significantly affect the transport properties of the fluid [36]. We also assume that the porous structure before an injection is homogenous. The effects of gravity, osmotic force, particle agglomeration, and the fluid exchange between the interstitial fluid and blood or lymph vessels on the fluid transport are not considered [5, 22]. Fluid flow and tissue deformation are considered steady state [33]. The solid phase of the medium is assumed as Hookian material, incompressible, isotropic, and fully saturated with fluid. The deformation during an infusion is infinitesimal. With these assumptions, the fluid flow through porous tissues is described by Darcy's equation [18].

$$\nabla \cdot (\varepsilon \mathbf{v}) = 0 \tag{1}$$

and

$$\nabla p_{\mathrm{f}} = -\frac{\varepsilon\mu}{\mathrm{K}}\mathbf{v} \tag{2}$$

where ε is the porosity, $\mathbf{v}$ is the interstitial fluid velocity vector, p_{f} is the fluid pressure, μ is the viscosity of the fluid, and K is the permeability of the tissue. The constitutive equation for tissue deformation is

$$\mathrm{G}\nabla^2\mathbf{u} + (\lambda + \mathrm{G})\nabla(\nabla \cdot \mathbf{u}) = \nabla(\varepsilon p_{\mathrm{f}}) \tag{3}$$

where $\mathbf{u}$ is the displacement vector, and G and λ are Lamé constants. Given Young's modulus E and Poisson's ratio υ, G and λ can be calculated using the following relationships: $\lambda = E\upsilon/((1 + \upsilon)(1 - 2\upsilon))$ and $G = E/(2(1 + \lambda))$.

During an infusion, backflow forms as the hydraulic pressure opens an annular space surrounding the needle outer surface. The bulk flow in the annular space is governed by the conservations of mass and momentum, which are

$$\begin{cases} \nabla \cdot \mathbf{v} = 0 \\ \mathbf{v} \cdot \nabla\mathbf{v} = -\frac{1}{\rho}\nabla p_{\mathrm{f}} + \frac{\mu}{\rho}\nabla^2\mathbf{v} \end{cases} \tag{4}$$

It should be noted that the porosity ε and permeability K in Eqs. 1–3 are variables that depend on tissue deformation; both are the functions of dilatation e, which is calculated by $e = \nabla \cdot \mathbf{u}$. When the volume of the solid phase of the porous medium is assumed unchanged for a small deformation, the porosity ε is computed by the expression [5, 6]

$$\varepsilon = \frac{\varepsilon_0 + e}{1 + e} \tag{5}$$

where ε_0 is the tissue porosity in the absence of deformation. Various empirical relationships have been proposed to quantify permeability K as a function of the dilatation e [9, 13, 19]. In this study, we employed a commonly used relation proposed by Lai and Mow [19] which prescribes an exponential increase in tissue permeability with dilatation e

$$K = K_0 \exp(Me) \tag{6}$$

where K_0 is the permeability in the absence of deformation, and M is a material constant that governs the variation of the permeability with the deformation. Typically M is related to tissue properties, densities of the cells, and extracellular matrix [5, 19, 22]. Through curve-fitting of the experimental data, previous studies suggest that M varies in the range of 0–5 [5, 19, 32]. We use a constant $M = 2$ in this study.

In order to predict the spreading shapes of the nanofluid, it is necessary to track the flow front of the nanofluid at the end of an infusion. In case of two immiscible fluids, the interface can be tracked using the color function method, where the fluid of interest is designated by a "color" function, i.e., $f = 1$. The equation for advection of f in the velocity field is then solved to track the position of the flow front, which is [24]

$$\frac{\partial f}{\partial t} + \nabla \cdot (\mathbf{v}f) = 0 \tag{7}$$

Although the nanofluid and water are miscible, the existing studies suggest that the diffusivities of nanoparticles in unbounded water are at the order of 10^{-11} m^2 s^{-1} [33]. Due to the low diffusivity, nanofluid injected in the agarose gel demonstrated a clear front and no obvious diffusion was observed within 24 h after an injection [30]. Therefore, we use the aforementioned interface tracking technique to study the nanofluid spreading in tumors.

The simulations of nanofluid injection in tumors are performed in a configuration depicted in Fig. 1, where a spherical tumor of 10 mm in diameter is embedded in 20 mm thick normal tissue. A needle is inserted at the center of the tumor. The boundary conditions used in this study are as follows: a finite pressure $p_{\mathrm{f}} = P_{\mathrm{inf}}$ is applied at the needle tip, and at the outer boundary where $r = R$, $p_{\mathrm{f}} = 0$. P_{inf} is adjusted so that it yields the desired infusion rate. No-slip condition is applied on the tissue and needle surfaces exposed to the backflow. For tissue deformation, a constant hydraulic pressure P_{inf} is applied on the needle tip, which yields

$$(2G + \lambda)\frac{\partial \mathbf{u}_z}{\partial z} = -P_{\mathrm{inf}} \tag{8}$$

At the outer boundary $r = R$, a fixed boundary condition $\mathbf{u} = 0$ is applied. The interface between the tissue and needle is considered deformable, which allows the tissue to recede from the needle surface. Major simulation parameters and tissue/tumor properties used in this study are given in Table 1.

The injection process is simulated by solving Eqs. 1–4 iteratively to determine the velocity field, the tissue deformation, and the length of the backflow in a two-

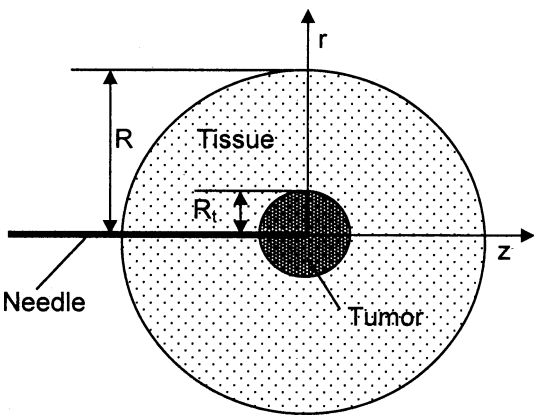

Fig. 1 Configuration for nanofluid injection in a tumor embedded in normal tissue ($R_{\mathrm{t}} = 5$ mm, $R = 25$ mm)

Table 1 Simulation parameters and tissue/tumor properties

Properties and parameters	Values
Injection amount	0.1 cc Ferrofluid
Particle diameter	10 nm
Needle	22, 26, and 32-Gauge, Hamilton needle
Injection rate	2.5–20 μl min^{-1}
Tissue porosity	0.4 [22]
Tumor porosity	0.2 [27]
Young's modulus of tissue (E)	60 kPa [7]
Young's modulus of tumor (E)	0.2–0.5 MPa [3, 5]
Initial tumor permeability	5×10^{-16} m^2 [5, 27]
Initial tissue permeability	1×10^{-14} m^2 [34]
Tissue/tumor Poisson's ratio	0.35 [5, 22]
Tumor diameter	10 mm [22]

dimensional axis-symmetric domain shown in Fig. 1. Once the velocity field is obtained, Eq. 7 is solved to track the front location of the nanofluid at the end of an injection. The injection duration is determined by the infusion amount and the injection rate. A commercially available multiphysics software COMSOL® is used to solve the equations. A total number of 22792 triangular elements with quadratic Lagrange shape functions are used in the simulation. Mesh dependency study is performed to insure the independency of the results on the number of the elements. Doubling the number of the elements resulted in less than 5% difference in the maximum velocity and tissue displacement.

3 Results

3.1 Effects of infusion rate

The formation of the backflow and the shape of the nanofluid distribution in a tumor embedded in the normal tissue are predicted using the poroelastic model. Figure 2a shows the predicted shape of the backflow on the needle outer surface for an infusion rate of 10 μl min^{-1}. It can be seen that under the hydraulic pressure, the tissue at the needle outer surface moves back, forming a nearly hemispherical cavity at the needle tip and an annular space that extends along a portion of the needle length. The infusate fills the space and forms the backflow. The formation of the backflow affects the nanofluid distribution substantially as shown in Fig. 2b. The infusate that fills the annulus infiltrates through the porous tissue in a direction perpendicular to the needle, thus distorting the spherical symmetry of the nanofluid distribution. Even for the infusion rates as low as 2.5 and 5 μl min^{-1}, the shapes of the nanofluid distribution

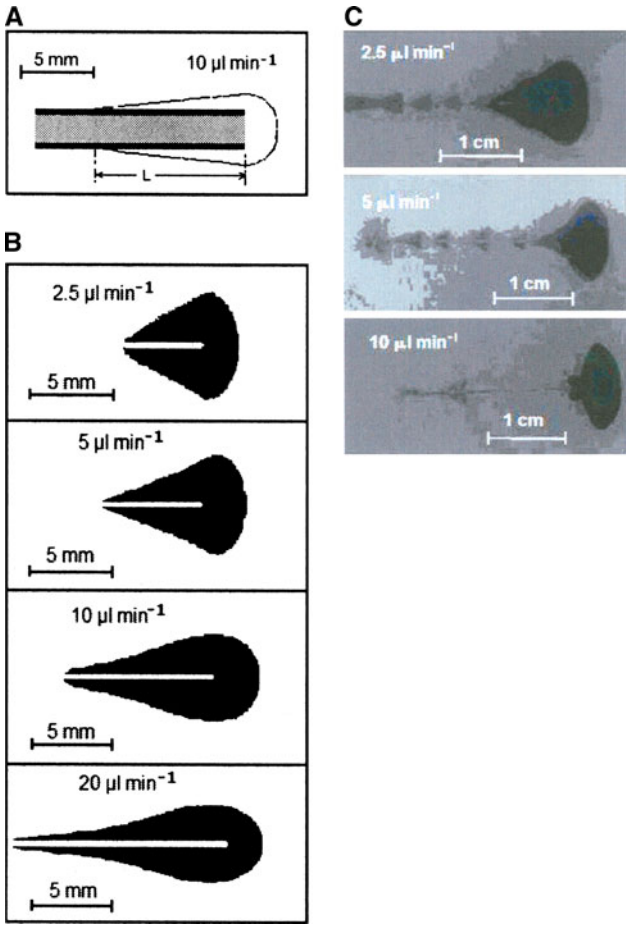

Fig. 2 **a** Tissue deformation at the needle outer surface for infusion rate of 10 μl min^{-1} (26-gauge, $E = 0.5$ MPa), L is the backflow length. The tissue deformation and needle diameter are magnified in the vertical direction for best visual effect. **b** Predicted shapes of the nanofluid spreading for various infusion rates (26-gauge, $E = 0.5$ MPa). **c** Shapes of the nanofluid distribution after injection 1% concentration gels [30]

volume are not spherical. However, these two infusion rates allow most of the infusate confined within the tumor. For high infusion rates in excess of 5 μl min^{-1}, the backflow length exceeds the tumor radius of 5 mm, and a leakage of the nanofluid into the normal tissue is possible. As a comparison, Fig. 2c gives the experimental images of the shapes of the ferrofluid spreading in agarose gels (1% concentration) for various injection rates [30]. Despite the different properties of tissues and gels, the predicted shapes of the nanofluid spreading at 2.5 and 5 μl min^{-1} are similar to those observed in the experiment. However, the simulation and the experimental results do not agree well for the injection rate of 10 μl min^{-1}. This discrepancy can be explained by the different mechanical responses of tissues and gels to hydraulic pressures. Typically, gels are more delicate with a lower tolerance to pressure than real tissues. Under a moderate infusion pressure, cracks may form in

gels in a plane perpendicular to the needle track, leading to extended bulk flow in that direction. The microCT imaging [2] confirms that the observed shape of the nanofluid distribution for the infusion rate of 10 μl min^{-1} is due to the formation of a crack in the gel. Real tissues, on the other hand, can sustain sufficiently high pressure elevation without a breakage. The infusion rate in real tumors reported in Ref. [35] varies in the range of 1.5–30 μl min^{-1}. Since our study focuses on the nanofluid transport in tumors, we choose infusion rates in the range of 5 – 20 μl min^{-1} in this study.

The length of the backflow depends on many factors including infusion rates, needle diameters, and tissue properties. Figure 3 shows the variations of the backflow length L with the infusion rate for various needle diameters. There is a clear indication that a faster infusion causes a longer backflow length due to the higher infusion pressure applied. Figure 4a shows the deformation-induced porosity distribution in the tumor for the infusion rate of 10 μl min^{-1} and 26-gauge needle. As the result of dilatation, a substantial increase of the porosity is observed not only near the tip, but also on the needle surface due to the backflow. Figure 4b shows the porosity profiles along the direction of injection for various infusion rates. Given the original tumor porosity of 0.2, a nearly 100% increase of the porosity is observed at the needle tip for a fast infusion rate of 20 μl min^{-1}. There is no substantial increase of the porosity for the infusion rate of 5 μl min^{-1}.

3.2 Effects of needle diameter

We studied the effect of the needle diameter on the backflow length using three different needles, 22, 26, and 32-gauge. The larger gauge needles have smaller diameters. Interestingly, a larger needle diameter yields a longer backflow length for all the infusion rates used in this study (Fig. 3), which subsequently causes more nanofluid to spread along the needle track (Fig. 5a). Figure 5b shows the porosity distribution along the direction of injection for various needle diameters for the injection rate of 10 μl min^{-1}. It is evident that a smaller needle diameter (32-gauge) yields a larger porosity, but the increased porosity is limited to a small region close to the needle tip. The effect of the dilatation is not substantial for 22-gauge needle.

3.3 Effects of tissue elastic properties

Previous studies of tissue mechanics reported that the elastic modulus of tissues varies over a wide range [3, 27]. In this study, the effects of tissue elastic properties on the backflow length, the shape of the nanofluid distribution, and the tissue porosity were studied by using various

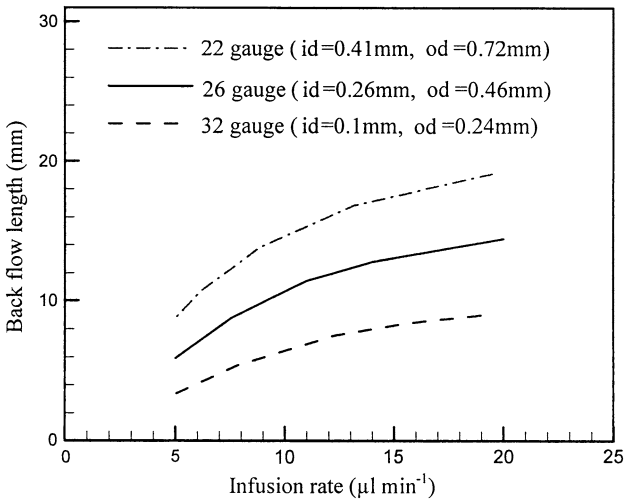

Fig. 3 Variations of backflow length with infusion rate for various needle diameters ($E = 0.5$ MPa)

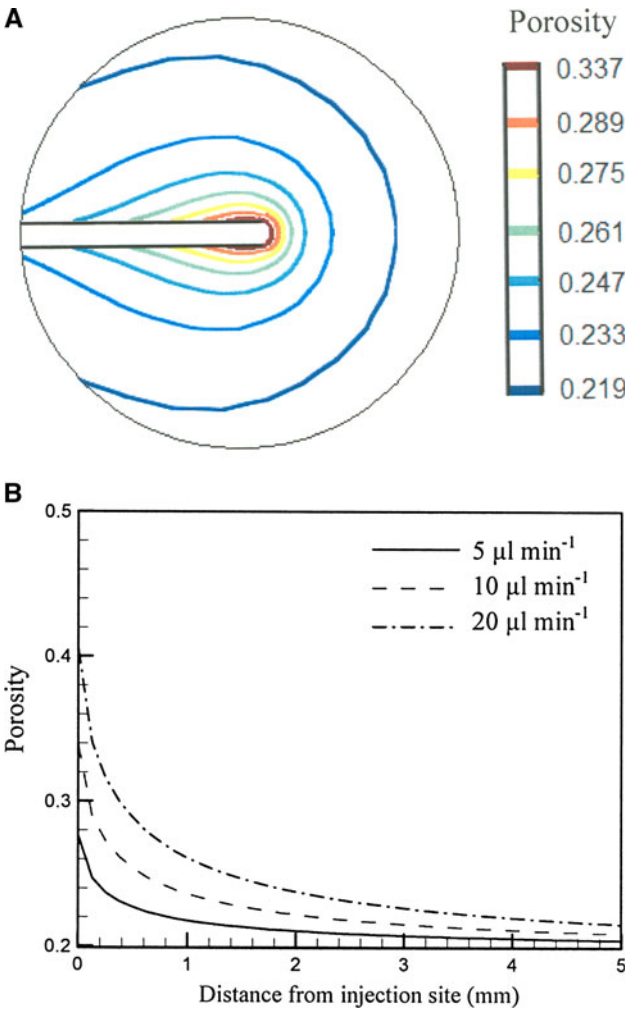

Fig. 4 **a** Porosity profile near the injection site within tumor for the infusion rate of 10 μl min^{-1} (26-gauge, $E = 0.5$ MPa). **b** Variations of porosity along the direction of injection for various infusion rates

E values in a range of 0.2–0.5 MPa. Figure 6a gives the variations of the backflow length with infusion rate for various values of E. It is evident that a flexible tissue is prone to deformation and yields a longer backflow length even at a low infusion rate of 5 μl min^{-1}. For an infusion in a stiff tissue, shorter backflow lengths are expected due to the large resistance to deformation. Figure 6b depicts the variations of the porosity along the direction of injection for the infusion rate of 10 μl min^{-1}. The increase of the tissue porosity in flexible tissue near the needle tip is evident.

4 Discussion

In hyperthermia cancer treatment using nanoparticles, it is preferable to have controlled nanoparticle distribution in tumors. This is especially important when multi-site injection is employed to cover large and/or irregular-shaped tumors. The distributions of nanofluids delivered from a point source or spherical cavity in an isotropic semi-infinite medium should be spherically symmetric. However, drugs delivered by direct infusion may exhibit different patterns of distribution due to the presence of the needle and the infusion-induced tissue deformation. Previous studies have identified that backflow may cause leakage of the infusate into healthy tissues and reduce the distribution volume of the infusate in the target region [1, 25]. The results from this study suggest that backflow length is also an important factor that defines the shapes of the nanofluid distribution volume. A higher infusion pressure creates a longer backflow distance, and thereby, yields a more irregular nanofluid spreading. For the tumor

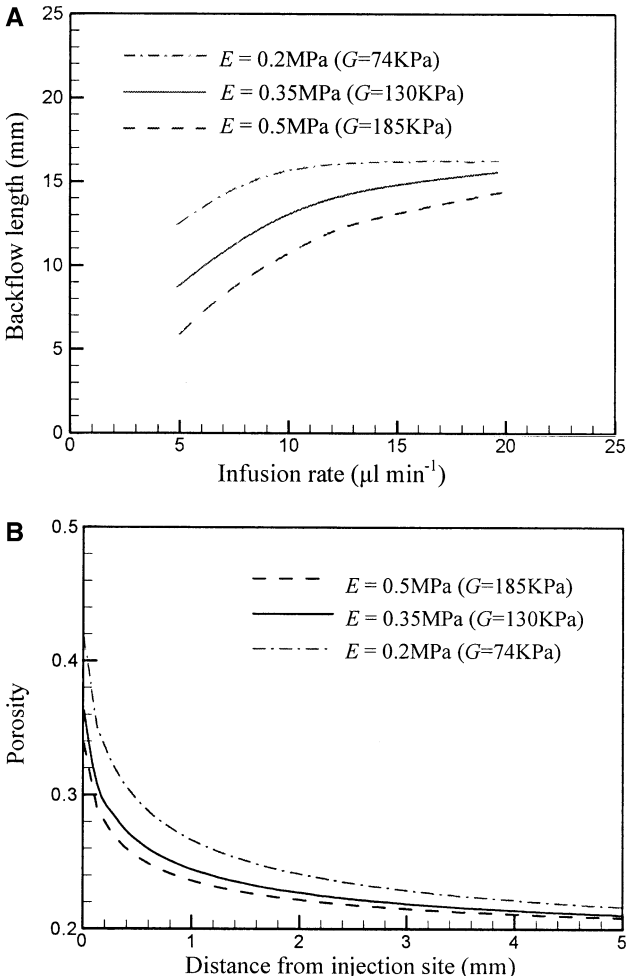

Fig. 6 **a** Variations of backflow length with infusion rate for various elastic tumor properties (26-gauge). **b** Variations of porosity along the direction of injection for various elastic tumor properties (10 μl min^{-1}, 26-gauge)

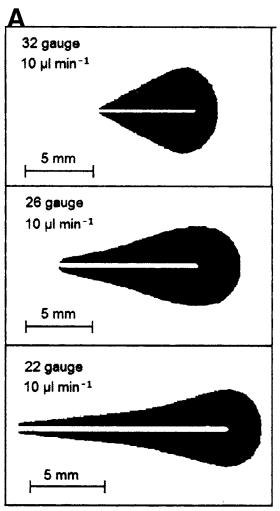

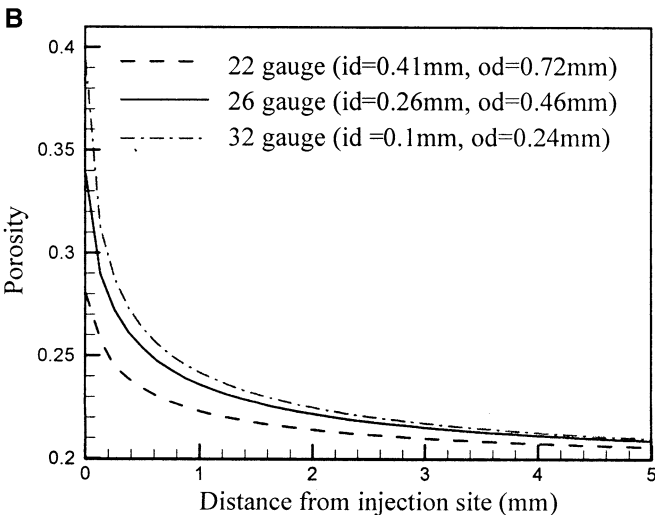

Fig. 5 **a** Predicted spreading shapes of the nanofluid for different needle diameters at 10 μl min^{-1} ($E = 0.5$ MPa). **b** Variations of porosity along the direction of injection for various needle diameters (10 μl min^{-1}, $E = 0.5$ MPa)

properties and injection parameters used in this study, a slow infusion rate (<10 μl min^{-1}) is recommended to avoid nanofluid leakage into the surrounding healthy tissue.

For a specific infusion rate, larger needle diameters are associated with slower infusion velocities at the needle tip, and subsequently, lower infusion pressures. Interestingly, a longer backflow length is observed for a larger needle diameter (Fig. 3). This observation is consistent with the study of infusion in brain tissues [25], which reported a monotonous increase of backflow length with needle diameter for infusion rates ranging from 0.03 to 5 μl min^{-1}. The relation between the backflow length and the needle diameter can be explained by the elastic deformation of a long thick cylindrical wall expanding radially outward under an annular pressure P_r. In this case, the radial deformation Δr is proportional to the radius r for a given P_r [25]

$$\Delta r = P_r \times r/2G \tag{9}$$

which suggests that a cylindrical wall of larger radius deforms more than a smaller one under the same annular pressure. Thereby, enlarging needle diameter creates competing effects on the backflow-reduced infusion pressure and larger tissue deformation in the radial direction. The observation of a longer backflow length for larger needle diameters suggests that the latter one dominates this process for the operational conditions used in this study.

Injection rate and needle diameter are two important parameters for a direct delivery of nanofluid. In order to confine heat generation in tumors, low infusion rates and small needle diameters should be used. However, a low infusion rate is associated with protracted injection duration, and a small needle diameter results in high pressures at the needle tip that may cause tumor breakage. Once cracks form in a tumor, the nanofluid flows through the cracks and makes it difficult to control its distribution. Accumulation of the infusate in the peripheral area of the tumor was observed at high infusion rates in a previous experimental study [35]. In addition, tumor properties should also be considered when selecting injection parameters. Strong backflow emerges even at low infusion rate in soft tissues. In summary, the knowledge of tumor size, tumor properties, as well as, the threshold at which tumor breaks under infusion pressures are critical for the design of an optimal injection protocol for a hyperthermia treatment.

Tissue deformation alters the pore size and porosity, which may substantially affect the penetration depth of therapeutic agents such as nanoparticles. Neeves et al. [26] demonstrated that nanoparticle penetration can be effectively improved by hydraulic dilation. Our simulation results show that a substantial increase of tumor porosity is observed near the needle tip for high infusion rates and small needle diameter (Figs. 4b, 5b). Thereby, enhanced penetration depths of the nanoparticles are anticipated in these circumstances. We also observe that the dilatation-influenced porosity is limited to a small area near the needle tip regardless of the infusion rate. Further study of the nanoparticle transport in tissues is needed to quantify the effect of tissue dilation on the particle distribution.

The poroelastic model developed in this study is limited to spherical, homogenous and isotropic tumors. In real tumors, the nanofluid distribution can be affected by other factors, including but not limited to the heterogeneous and anisotropic tumor properties, irregular tumor shapes, cracks and necrotic tissues which are common features in large tumors. In addition, elevated infusion pressure may break tumors and cause the formation of cracks during an infusion process. These mechanisms should be included in the model in future studies. Besides, this model does not consider the increased viscosity of the infusate with dispersed nanoparticles, thus is limited to dilute nanofluids. However, ferrofluids of low concentrations have been used in hyperthermia treatment with positive outcome. The in vivo animal study by Salloum et al. [31] has demonstrated that 0.2 cc of 3.3 vol.% ferrofluid generates sufficient level of heat to elevate the tissue temperature above 43°C. Also, the first clinical hyperthermia by Johannsen et al. [16] used a particle concentration of 120 mg/ml, which corresponds to a volumetric concentration of 2.29%. The change of the rheological behaviors of nanofluids should be considered for moderate or high concentration nanofluids, and the effects of particle concentration on flow pattern and backflow length should be investigated in future study.

In summary, tissue deformation is identified as the leading mechanism causing the irregular-shaped nanofluid spreading, and can facilitate particle penetration in tumors. Low infusion rate and small needle diameter are recommended to reduce the backflow. The design of an optimal infusion protocol requires the consideration of the tumor properties, heterogeneous structure of tumors, and the information on the tumor breakage under infusion pressure. The study presented in this article is the first step toward a systematic simulation of nanoparticle transport during an infusion process in hyperthermia applications. The information obtained in this study on nanofluid velocity field, tissue deformation, and pore swelling will be used for the simulation of nanoparticle convection and deposition in tissue where the size and properties of the particles play a critical role.

Acknowledgment This research is supported by NSF research grant CBET-0828728.

References

1. Allard E, Passirani C, Benoit JP (2009) Convection-enhanced delivery of nanocarriers for the treatment of brain tumors. Biomaterials 30(12):2302–2318
2. Attaluri A, Ma R, Zhu L (2011) Using microCT imaging technique to quantify heat generation distribution induced by magnetic nanoparticles for cancer treatments. J Heat Transf 133(1): 011003–011005
3. Basser PJ (1992) Interstitial pressure, volume, and flow during infusion into brain tissue. Microvasc Res 44:143–165
4. Bernardi RJ, Lowery AR, Thompson PA, Blaney SM, West JL (2008) Immunonanoshells for targeted photothermal ablation in medulloblastoma and glioma: an in vitro evaluation using human cell lines. J Neurooncol 86:165–172
5. Chen XM, Sarntinoranont M (2007) Biphasic finite element model of solute transport for direct infusion into nervous tissue. Annu Biomed Eng 35(12):2145–2158
6. Chen ZJ, Broaddus WC, Viswanathan RR, Raghavan R, Gillies GT (2002) Intraparenchymal drug delivery via positive-pressure infusion: experimental and modeling studies of poroelasticity in brain phantom gels. IEEE Trans Biomed Eng 49(2):85–96
7. Choi APC, Zheng YP (2005) Estimation of Young's modulus and Poisson's ratio of soft tissue from indentation using two different-sized indentors: finite element analysis of the finite deformation effect. Med Biol Eng Comput 43(2):258–264
8. El-Sayed IH, Huang X, El-Sayed MA (2006) Selective laser photothermal therapy of epithelial carcinoma using anti-EGFR antibody conjugated gold nanoparticles. Cancer Lett 239:129–135
9. Gu WY, Hao H, Huang CY, Cheung HS (2003) New insight into deformation-dependent hydraulic permeability of gels and cartilage, and dynamic behavior of agarose gels in confined compression. J Biomech 36(4):593–598
10. Hergt R, Hiergeist R, Zeisberger M, Glockl G, Weitschies W, Ramirez LP, Hilger I, Kaiser WA (2004) Enhancement of AC-losses of magnetic nanoparticles for heating applications. J Magn Magn Mater 280:358–368
11. Hilger I, Andra W, Hergt R, Hiergeist R, Schubert H, Kaiser WA (2001) Electromagnetic heating of breast tumors in interventional radiology: in vitro and in vivo studies in human cadavers and mice. Radiology 218(2):570–575
12. Hilger I, Hergt R, Kaiser WA (2005) Towards breast cancer treatment by magnetic heating. J Magn Magn Mater 293(1): 314–319
13. Holmes MH, Mow VC (1990) The nonlinear characteristics of soft gels and hydrated connective tissues in ultrafiltration. J Biomech 23(11):1145–1156
14. Ivanchenko O, Sindhwani N, Linninger A (2010) Experimental techniques for studying poroelasticity in brain phantom gels under high flow microinfusion. J Biomech Eng 132(5):051008
15. Jain RK (1997) Delivery of molecular and cellular medicine to solid tumors. Adv Drug Deliv Rev 26(2–3):71–90
16. Johannsen M, Gneveckow U, Eckelt L, Feussner A, Waldofner N, Scholz R, Deger S, Wust P, Loening SA, Jordan A (2005) Clinical hyperthermia of prostate cancer using magnetic nanoparticles: presentation of a new interstitial technique. Int J Hyperth 21:637–647
17. Jordan A, Scholz R, Maier-Hauff K, Van Landeghem FK, Waldoefner N, Teichgraeber U, Pinkernelle J, Bruhn H, Neumann F, Thiesen B, Von Deimling A, Felix R (2006) The effect of thermotherapy using magnetic nanoparticles on rat malignant glioma. J Neuro-Oncol 78:7–14
18. Khaled A-RA, Vafai K (2003) The role of porous media in modeling flow and heat transfer in biological tissues. Int J Heat Mass Transf 46(26):4989–5003
19. Lai WM, Mow VC (1980) Drug-induced compression of articular cartilage during a permeation experiment. Biorheology 17:111–123
20. Lim CT, Han J, Guck J, Espinosa H (2010) Micro and nanotechnology for biological and biomedical applications. Med Biol Eng Comput 48(10):941–943
21. Matsuki H, Yanada T, Sato T, Murakami K, Minakawa S (1994) Temperature-sensitive amorphous magnetic flakes for intratissue hyperthermia. Mater Sci Eng A181(182):1366–1368
22. McGuire S, Zaharoff D, Yuan F (2006) Nonlinear dependence of hydraulic conductivity on tissue deformation during intratumoral infusion. Annu Biomed Eng 34(7):1173–1181
23. Moroz P, Jones SK, Gray BN (2002) Magnetically mediated hyperthermia: current status and future directions. Int J Hyperth 18(4):267–284
24. Morris JP (2000) Simulating surface tension with smoothed particle hydrodynamics. Int J Numer Methods Fluids 33:333–353
25. Morrison PF, Chen MY, Chadwick RS, Lonser RR, Oldfield EH (1999) Focal delivery during direct infusion to brain: role of flow rate, catheter diameter, and tissue mechanics. Am J Physiol 277(4):R1218–R1229
26. Neeves KB, Sawyer AJ, Foley CP, Saltzman WM, Olbricht WL (2007) Dilation and degradation of the brain extracellular matrix enhances penetration of infused polymer nanoparticles. Brain Res 1180:121–132
27. Netti PA, Baxter LT, Boucher Y (1997) Macro- and microscopic fluid transport in living tissues: application to solid tumors. AIChE J 43(3):818–834
28. O'Neal DP, Hirsch LR, Halas NJ, Payne JD, West JL (2004) Photo-thermal tumor ablation in mice using near infrared-absorbing nanoparticles. Cancer Lett 209:171–176
29. Raghavan R, Mikaelian S, Brady M, Chen ZJ (2010) Fluid infusions from catheters into elastic tissue: I. Azimuthally symmetric backflow in homogeneous media. Phys Med Biol 55: 281–304
30. Salloum M, Ma R, Weeks D, Zhu L (2008) Controlling nanoparticle delivery in magnetic nanoparticle hyperthermia for cancer treatment: experimental study in agarose gel. Int J Hyperth 24(4):337–345
31. Salloum M, Ma R, Zhu L (2008) An in vivo experimental study of temperature elevations in animal tissue during magnetic nanoparticle hyperthermia. Int J Hyperth 24(7):589–601
32. Sobey I, Wirth B (2006) Effect of non-linear permeability in a spherically symmetric model of hydrocephalus. Math Med Biol 23(4):339–361
33. Su D, Ma R, Salloum M, Zhu L (2010) Multi-scale study of nanoparticle transport and deposition in tissues during an injection process. Med Biol Eng Comput 48:853–863
34. Swartz MA, Fleury ME (2007) Interstitial flow and its effects in soft tissues. Annu Rev Biomed Eng 9:229–256
35. Wang Y, Wang H, Li C-Y, Yuan F (2006) Effects of rate, volume, and dose of intratumoral infusion on virus dissemination in local gene delivery. Mol Cancer Ther 5(2):362–366
36. Warszynski P (2000) Coupling of hydrodynamic and electric interactions in adsorption of colloidal particles. Adv Colloid Interface Sci 84(1–3):47–142